PTEP

Prog. Theor. Exp. Phys. **2020**, 123G01 (12 pages)
DOI: 10.1093/ptep/ptaa111

Polarized proton spin filter for epithermal neutrons based on dynamic nuclear polarization using photo-excited triplet electron spins

Shusuke Takada[1,2,*], Kenichiro Tateishi[1,3], Yasuo Wakabayashi[4], Yoshimasa Ikeda[4], Tamaki Yoshioka[5], Yoshie Otake[4], and Tomohiro Uesaka[1,3]

[1]*Cluster for Pioneering Research, RIKEN, 2-1 Hirosawa, Wako, Saitama 351-0198, Japan*
[2]*Department of Physics, Kyushu University, 744 Motooka, Nishi, Fukuoka 819-0395, Japan*
[3]*Nishina Center for Accelerator-Based Science, RIKEN, 2-1 Hirosawa, Wako, Saitama 351-0198, Japan*
[4]*RIKEN Center for Advanced Photonics, RIKEN, Wako, Saitama 351-0198, Japan*
[5]*Research Center for Advanced Particle Physics, Kyushu University, 744 Motooka, Nishi, Fukuoka 819-0395, Japan*
*E-mail: takada@epp.phys.kyushu-u.ac.jp

Received April 25, 2020; Revised July 10, 2020; Accepted July 18, 2020; Published July 21, 2020

To polarize neutrons with energy beyond 0.1 eV, we developed a novel polarized proton spin filter based on dynamic nuclear polarization using photo-excited triplet electron spins. The spin filter consists of a single crystal of naphthalene doped with deuterated pentacene and has a size of $\varnothing 15 \times 4\ \mathrm{mm}^3$, allowing it to cover a wide beam diameter. It was operated in 0.35 T and at 90 K. We succeeded in polarizing neutrons in the energy range 0.1–10 eV using a RIKEN accelerator-driven compact neutron source. The averaged values of the proton and neutron polarization were 0.250 ± 0.050 and 0.076 ± 0.015, respectively.

Subject Index C03, G12

1. Introduction

Polarized neutrons have a wide range of values in physics and in industry. Notably, polarized epithermal neutrons with energy in the range 0.1–1000 eV are useful mainly for studies on neutron-induced compound states which are formed by neutron capture when the epithermal neutron beam is injected into a nucleus target. One area of study using compound states involves the search for time-reversal (T) violation, which is an open question in elementary particle physics to explain the development of the universe. T-violation search with compound states can allow studies for new physics beyond the standard model of elementary particles, e.g. supersymmetry [1–3]. In the compound states, extremely large helicity dependence of the capture cross-sections has been observed in various nuclei [4]. These helicity dependencies have proved the existence of parity (P) violations in the compound states that are 10^6 times larger than in proton–proton scattering. The large P-violation is theoretically explained as interference between s- and p-wave resonances. Moreover, the T-violation with compound states may also be enhanced by a similar mechanism [2]. T-violation search is performed with a polarized epithermal neutron beam and a polarized nucleus target.

Neutron spin filters are devices for neutron beam polarization that rely on the spin-dependent cross-section of nuclear capture in polarized ^{3}He nuclei or scattering on polarized protons. The former is now available at several neutron facilities; however, it is impossible to optimize the filter size for

a wide energy range because the capture cross-section decreases rapidly in the epithermal region. The latter is currently the only idea for neutron polarization with energies up to keV, because the neutron–proton scattering cross-section is nearly constant in the epithermal region. The polarized proton spin filter was first demonstrated by Lushchikov et al. using the method of dynamic nuclear polarization (DNP) [5]. In this method, electron polarization is transferred to a proton via microwave irradiation for polarizing proton spins in solids [6,7]. DNP relies on the thermally equilibrated high polarization of electrons, which is added to samples as polarizing agents and is realized at cryogenic temperatures ($\sim$1 K) and with a strong magnetic field (2.5–5 T). In addition to the foregoing strict environment, because the flux of the thermal neutron (meV–eV) is higher than that of the epithermal neutron in most pulsed neutron sources, the polarized ^{3}He spin filter has become preferred over the polarized proton spin filter.

Recently, the polarized proton spin filter has again been in demand because the fluxes of epithermal neutrons are increasing at neutron facilities, e.g. the Japan Proton Accelerator Research Complex (J-PARC). In the meantime, an alternative method for polarizing protons has been developed. This method is called DNP with photo-excited triplet electron spins (triplet DNP), wherein non-equilibrated electron spins are utilized. A selection rule determines the polarization of the triplet electron in the intersystem crossing, independent of temperature and magnetic field strength. Neutron polarization is realized with a simple setup because of the milder environment compared to that of conventional DNP, so that a polarized proton spin filter based on triplet DNP (triplet-DNP spin filter) can be installed in existing beamlines. Since the magnetic field leakage is small due to the milder field, the experimental equipment, e.g. nucleus target and detector, can be set near to each other in a beamline. Since the spin filter and the detector can be placed close together, we can use the neutron beam before diverging it. The pioneering work on the triplet-DNP spin filter was first conducted at the Paul Scherrer Institut (PSI) in Switzerland [8–11]. They achieved a proton polarization of 0.80 at 25 K and in 0.36 T, using a single crystal of naphthalene doped with deuterated pentacene with a size of $5 \times 5 \times 5\,\mathrm{mm}^3$. They applied it to cold neutrons and carried out a small-angle neutron scattering (SANS) experiment [12]. However, the triplet-DNP spin filter has never been applied to epithermal neutrons.

This paper reports the first demonstration of the polarization of epithermal neutrons with a triplet-DNP spin filter. First, the working principles of polarized proton spin filters are reviewed in Sect. 2, and the optimal thickness of a triplet-DNP spin filter for the epithermal region is discussed. In Sect. 3, we describe the experimental setup for neutron transmission using a triplet-DNP spin filter and a neutron beam. Considering the triplet-DNP spin filter, a single crystal of naphthalene doped with deuterated pentacene was used with a size of $\varnothing 15 \times 4\,\mathrm{mm}^3$. Thereafter, triplet DNP was carried out at 90 K and in 0.35 T. The performance of the triplet-DNP spin filter was evaluated by comparing the neutrons passing through the triplet-DNP spin filter with and without proton polarization. The evaluation of the performance is described in Sect. 4. Section 4 provides a comparison with the polarized ^{3}He spin filter and future improvements thereon. The neutron transmission experiment was conducted using the RIKEN accelerator-driven compact neutron source (RANS) [13]. RANS provides a pulsed neutron beam with a wide energy region from meV to MeV. Sufficient neutron beam intensity for the evaluation could be obtained by optimizing the experimental setup. Proton polarization was kept for 70 hr without radiation damage. Neutron polarization in the epithermal region was clearly observed.

2. Design of triplet-DNP spin filter for epithermal neutrons

The triplet-DNP spin filter is based on the polarization of the hydrogen nuclei contained in a naphthalene crystal. The principle of neutron polarization with the polarized proton spin filter relies on the fact that the singlet cross-section for neutron–proton scattering is twenty times larger than the triplet cross-section [5,14]. The total cross-section of neutron–proton scattering is customarily defined as the sum of the spin-dependent and spin-independent cross-sections ($\sigma_{\rm p}$ and σ_0) [7,15,16]:

$$\sigma = \sigma_0 + \sigma_{\rm p} P(\boldsymbol{S} \cdot \boldsymbol{I}), \tag{1}$$

where P is the proton polarization, and $\boldsymbol{S}$ and $\boldsymbol{I}$ are the unit vectors of the incident neutron spin and the proton spin, respectively. Thus, neutrons that are polarized anti-parallel to the protons will interact much more strongly compared to those that are polarized parallel. Considering that the main component of the triplet-DNP spin filter is naphthalene, an unpolarized neutron beam is exponentially attenuated by passing through it with the proton and carbon densities n and $n_{\rm C}$, respectively, and filter thickness d. The neutron transmission of the polarized and unpolarized proton spin filter ($T_{\rm n}$ and $T_{\rm n0}$) are expressed using the following equations:

$$T_{\rm n0} = \exp\{-(n\sigma_0 + n_{\rm C}\sigma_{\rm C})\, d\}, \tag{2}$$

$$T_{\rm n} = \exp\{-(n\sigma_0 + n_{\rm C}\sigma_{\rm C})\, d\} \cosh\left(n\sigma_{\rm p} P d\right), \tag{3}$$

$$\frac{T_{\rm n}}{T_{\rm n0}} = \cosh\left(n\sigma_{\rm p} P d\right), \tag{4}$$

where σ_0 and $\sigma_{\rm C}$ are the cross-sections of neutron scattering with the unpolarized proton and the carbon nucleus, respectively. The neutron polarization $P_{\rm n}$ after passing through the spin filter is written as [14]

$$P_{\rm n} = \tanh\left(n\sigma_{\rm p} P d\right). \tag{5}$$

A figure of merit (FOM) is taken as the statistically relevant factor in the optimization of the spin filter performance [17], and it is defined by the following equation:

$$\mathrm{FOM} = P_{\rm n}^2 T_{\rm n}. \tag{6}$$

The performance of the triplet-DNP spin filter in the epithermal region is calculated using Eq. (6) as a function of the filter thickness d. Figure 1 shows the neutron polarization, the neutron transmission, and the FOM for the $P = 0.1$, 0.3, and 0.5 cases. Here, $n_{\rm p} = 4.29 \times 10^{22}\,/\mathrm{cm}^3$, $n_{\rm C} = 5.36 \times 10^{22}\,/\mathrm{cm}^3$, $\sigma_0 = 20.5$ barn, $\sigma_{\rm p} = 16.7$ barn, and $\sigma_{\rm C} = 4.74$ barn were used. A thicker filter leads to higher neutron polarization and lower transmission. The optimum thickness is $\sim$15 mm. Moreover, it is almost independent of the proton polarization.

Triplet DNP using a single crystal of naphthalene was originally demonstrated by Henstra et al. in 1990 [18]. This method has a substantial advantage over DNP with radicals. It enables the production of nuclear hyperpolarization at a relatively lower magnetic field and a higher temperature. This can reduce the stray magnetic field, and makes expensive and high-tech cryogenic devices unnecessary. A proton polarization of 0.80 has been obtained at 25 K and in 0.36 T [11]; 0.34 has been achieved even at room temperature and in 0.40 T [19]. Recently, this method has been applied not only in accelerator science but also in the chemical and medical fields [20–22].

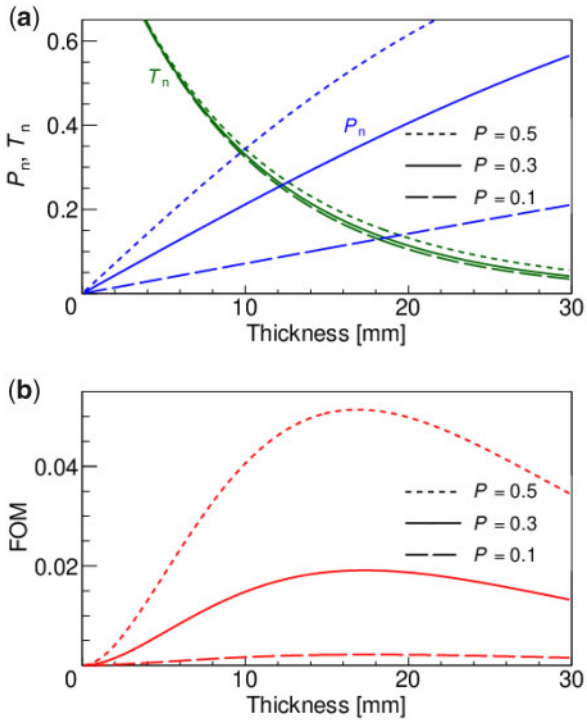

Fig. 1. Performance of the polarized proton spin filter with proton polarization $P = 0.1$, 0.3, and 0.5 for epithermal neutrons. (a) Degree of neutron polarization (P_n) and neutron transmission (T_n) as a function of spin filter thickness. (b) Figure of merit (FOM) as a function of spin filter thickness.

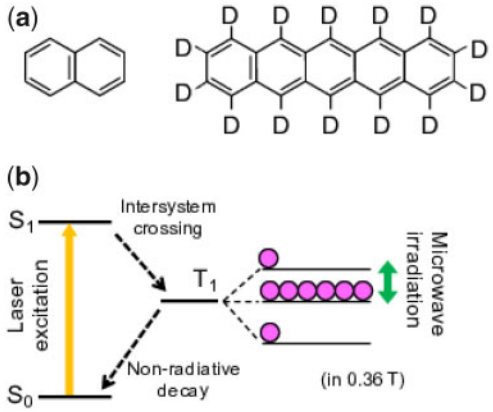

Fig. 2. (a) Naphthalene (left) and deuterated pentacene (right) molecule. (b) Simplified energy diagram of pentacene showing a pathway during triplet DNP.

We applied triplet DNP to a single crystal of naphthalene doped with 0.003 mol% deuterated pentacene, Fig. 2(a). The triplet DNP polarization procedure, which is explained in Ref. [23], begins with laser irradiation to generate hyperpolarized electrons. Figure 2(b) shows the energy diagram of pentacene. Light irradiation with a wavelength of 589 nm induces the transition from its ground singlet state S_0 to its excited triplet state T_1 via its excited singlet state S_1. The transition probability determines the population of the triplet state. In the case of pentacene, the populations are 0.045, 0.910, and 0.045, which corresponds to an electron polarization of 0.906 when the long axis of the molecule is aligned parallel to the external magnetic field [24]. The hyperpolarization of triplet

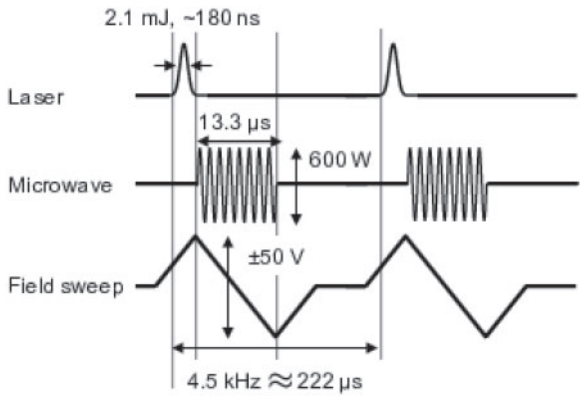

Fig. 3. Pulse sequence of triplet DNP. One cycle is composed of a laser pulse for generating a hyperpolarized triplet electron, and a microwave pulse and a field sweep for polarization transfer.

electrons is transferred to nearby protons during the lifetime of the electron through the process called the integrated solid effect (ISE) [25]. Figure 3 shows a cycle of the ISE. In the ISE, a magnetic field sweep and microwave irradiation are applied simultaneously. The inhomogeneously broadened electron spin packets are swept adiabatically. We found that the Rabi frequency of the electron spin in the rotating system matches the Larmor frequency of the proton spin at some point in the adiabatic process. The excited electrons decay non-radiatively to S_0, and the hyperpolarized spin state diffuses to the whole naphthalene crystal. By repeating this cycle, the proton polarization can be accumulated until the buildup and proton spin-lattice relaxation are balanced.

Triplet DNP was conducted in 0.35 T using a C-type electromagnet with a gap of 100 mm and a pole diameter of 220 mm. The resonance frequencies of electron and proton were 9.2 GHz and 15.0 MHz (high-field transition), respectively. A diode-pumped solid-state (DPSS) laser (CNI, HPL-589-Q) was used for pentacene excitation. The wavelength, pulse width, pulse energy, and repetition rate were 589 nm, ∼180 ns, 2.1 mJ, and 4.5 kHz, respectively. The laser pulses were sampled with a photodiode and converted to TTL level. The signals were used as a trigger for the subsequent microwave and field sweep. A microwave pulse amplified to 600 W using a pulsed travelling wave tube amplifier (IFI, PT188-1KW, max duty 6%), with a width of 13.3 μs, was applied, while the field was adiabatically swept with a voltage of ±50 V. The transmission loss was around −3 dB. The polarized proton signals were monitored using an OPENCORE nuclear magnetic resonance (NMR) spectrometer [26,27].

The triplet DNP system was set in a double-walled chamber (Fig. 4(a)). The inner chamber was cooled to 90 K using cooled nitrogen gas, and the outer chamber was kept at ∼20 Pa to prevent frosting. Optical windows were attached to the chambers. The laser light was introduced from three places: one from upstream and two from downstream. For the upstream, a dielectric-coated silicon substrate mirror with a thickness of 1 mm was used to minimize the neutron transmission loss. The inside of the chamber is shown in Fig. 4(b). The naphthalene crystal was placed at the center of the electromagnet.

The crystal was cut to the size of $\varnothing 15 \times 4\,\mathrm{mm}^3$ because the power of our laser was insufficient to polarize the 15 mm-thick filter. It was mounted on a Teflon holder. A TE_{011} cylindrical cavity equipped with a field-sweep coil and a split-coil for NMR was utilized. The diameter and length were 21 mm and 25 mm, respectively. A coaxial microwave transmission line was adapted to a

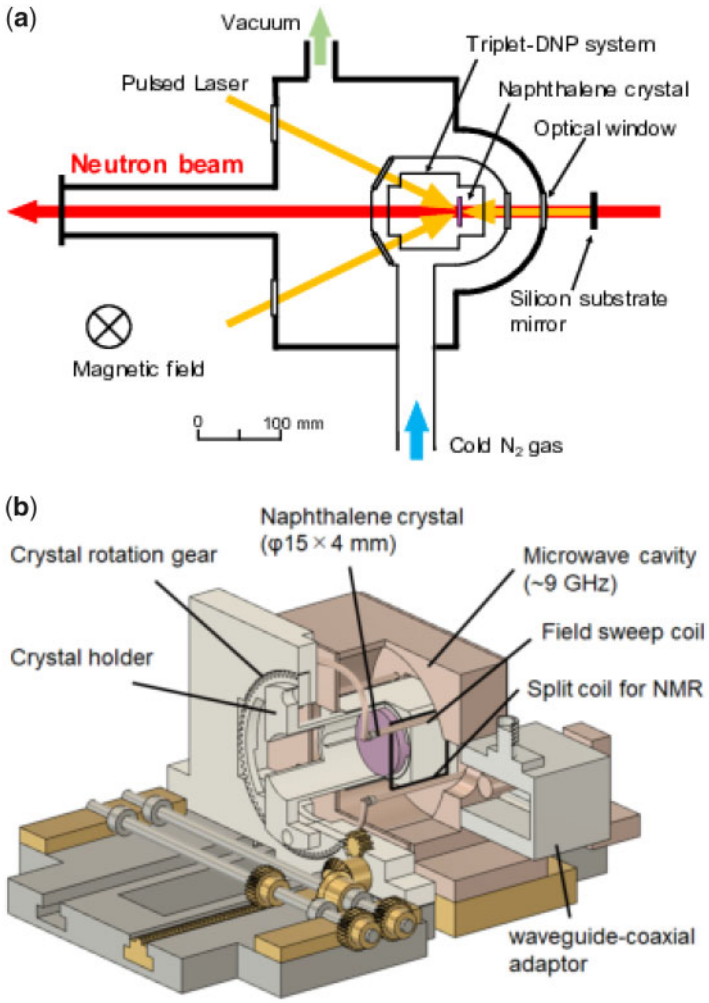

Fig. 4. (a) Experimental setup of triplet DNP. A double-walled chamber is put in an electromagnet. The inner chamber was cooled to 90 K, and the outer chamber was kept at ∼20 Pa. Lasers were irradiated from three lines. (b) A schematic of the home-built TE_{011} cylindrical cavity equipped with a field-sweep coil and a split-coil for NMR. The naphthalene crystal can be rotated using the crystal rotation gear.

waveguide and coupled with the cavity through an iris. The crystal could be rotated using a crystal rotation gear. Moreover, its alignment could be adjusted precisely.

3. Optical layout for transmission experiment

The performance of the triplet-DNP spin filter was tested by measuring neutron transmission with RANS. RANS is a compact neutron source which has been in operation since 2013 and has been applied to the development of non-destructive inspection methods for infrastructure and industrial products, e.g. concrete and steel [28–32]. RANS consists of a linear accelerator and a target station, as shown in Fig. 5(a). Protons are accelerated to 7 MeV and injected into a beryllium target [28]. Neutrons with a maximum energy of ∼5 MeV are generated via the ^{9}Be (p,n) reaction. The neutrons are slowed down through a 40 mm-thick polyethylene moderator and extracted from the target station. An energy spectrum at a position 5 m from the Be target is shown in Ref. [13]. The Be target and the moderator are surrounded with carbon blocks as a neutron reflector, borated polyethylene

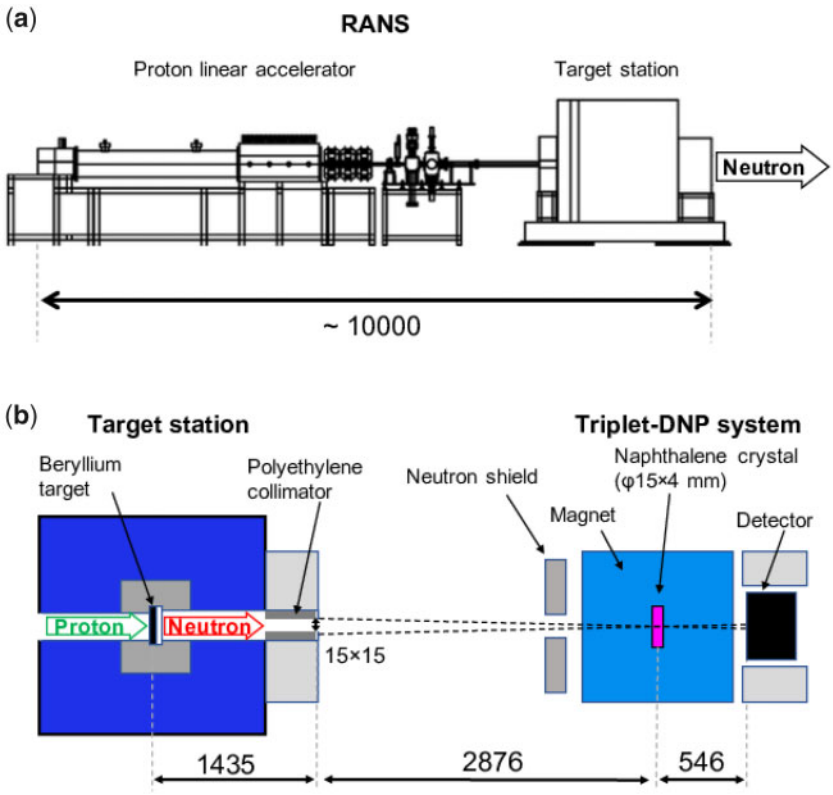

Fig. 5. (a) Side view of RANS. (b) Top view of the setup for the neutron transmission experiment with RANS.

(BPE) powder in aluminum boxes, and lead blocks in iron enclosures as a shield for neutrons and gamma-rays.

The experimental setup is shown in Fig. 5(b). A 10% BPE collimator with a hole of $15 \times 15\,\mathrm{mm}^2$ was installed at the RANS target station. A neutron shield for reducing the background signal consists of BPE blocks and boron rubber sheets. A resistor-type photomultiplier tube (RPMT) detector, which consists of a ZnS(Li) scintillator and a position-sensitive photomultiplier tube [33], was used for measuring the two-dimensional position and neutron time of flight (TOF). The detector was set in an aluminum box with BPE powder to shield background neutrons, and placed 0.55 m behind the naphthalene crystal. At that position, the stray field from the electromagnet was less than 10 G, and it did not affect the photomultiplier tube of the detector. The spatial resolution and the neutron beam intensity are functions of the distance from the neutron source to the spin filter. The longer the distance, the better the spatial resolution, but the smaller the neutron beam intensity. The distance was set to be 4.31 m, and the resolution and the intensity in the whole energy region were roughly 2 mm, and 8.3×10^5 count hr^{-1}, respectively.

The neutron pulse structure determines the maximum and minimum available neutron energy. A shorter pulse width leads to a higher maximum available neutron energy, but a smaller neutron beam intensity. In this experiment, the pulse width and repetition rate were set at 60 μs and 105 Hz, respectively. Considering the repetition rate and the distance from the Be target to the detector, the minimum available neutron energy was 1 meV. We performed a measurement without a target to calculate the neutron transmission (blank measurement). In order to subtract unexpected events, such as a scattering with a microwave cavity, we carried out a measurement with a boron rubber target (33 mm thickness) instead of the naphthalene crystal (background measurement). Figure 6

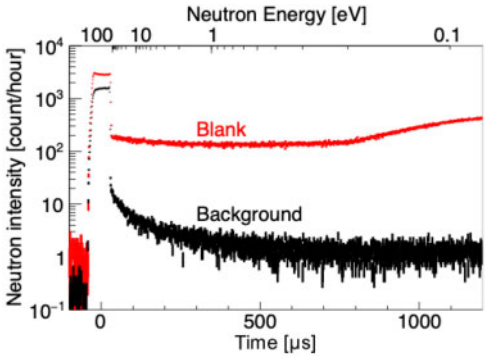

Fig. 6. Neutron beam intensity of blank and background measurements in the epithermal region as a function of the time of flight.

shows the epithermal region of the TOF spectra with the blank measurement and the background measurement. The neutron beam intensity of the background measurement is 10–10^2 lower than the corresponding blank measurement for all time regions in the TOF spectrum. Considering the pulse width and the distance from the Be target to the detector, the maximum available neutron energy was 10 eV. The TOF signals for the full range are shown in Supplementary Fig. S1. The neutron beam intensity was 1.7×10^5 count hr^{-1} in the 0.1–10 eV range.

4. Neutron polarization experiment

The relative magnitude of the proton polarization was monitored using the NMR method mentioned in Sect. 3. Figure 7 shows the intensities of the NMR signals recorded during the beamtime. An expanded version of Fig. 7 for 0–15 hr is shown in Supplementary Fig. S2; the buildup time was about 2.5 hr. The shaded areas show the irradiation time of the neutron beam. We irradiated the neutron beam after the buildup of the proton polarization was fully saturated. Radiation damage was not observed because the signal intensity did not decrease during the neutron irradiations. The protons were depolarized at around $T = 80$ hr, and this state was maintained. The depolarized state was realized by shifting the relative timing of the microwave and the field sweep to the laser instead of cutting off the polarization sequence shown in Fig. 3 in order to keep the environment inside the inner chamber. At the offline measurement, the relaxation time in the irradiation of the laser was 5.8 hr (shown in Supplementary Fig. S2). Using the buildup constant and the relaxation time obtained from the NMR results, the proton polarization was calculated to be 51.2%. However, an unpolarized area due to the lack of laser power is not included in the above estimation. The total proton polarization has to be measured by using neutrons.

An absolute value for the proton polarization is analyzed from comparing the neutrons pass through the triplet-DNP spin filter with and without proton polarization. Figure 8 shows the ratio of the TOF spectrum with and without proton polarization of the naphthalene crystal, which is consistent with the ratio of neutron transmission $T_\mathrm{n}/T_\mathrm{n0}$. Here, the TOF is converted to a neutron energy E_n by

$$E_\mathrm{n} = \frac{m_\mathrm{n}}{2}\left(\frac{L}{t}\right)^2, \tag{7}$$

where m_n is the neutron mass, L is the distance between the Be target and the RPMT detector, and t is the TOF. The ratio of the neutron transmission $T_\mathrm{n}/T_\mathrm{n0}$ as a function of neutron energy is reasonable according to Eq. (4) because the ratio is greater than one over the whole region, as shown

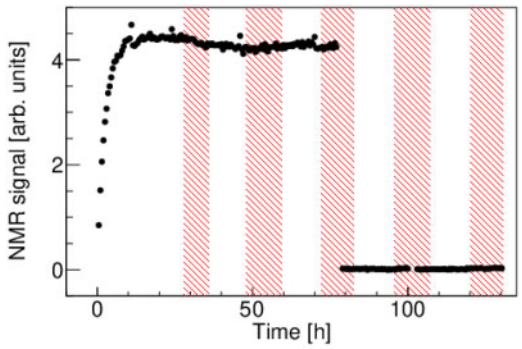

Fig. 7. Relative intensity of the proton polarization during the beamtime. The shaded areas pertain to the neutron irradiations.

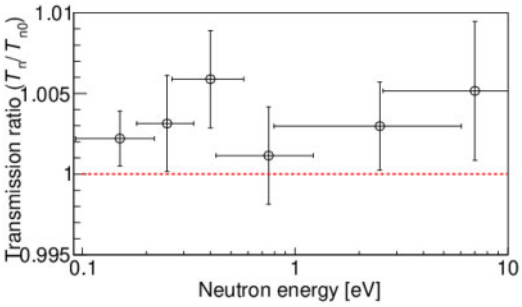

Fig. 8. Ratio of neutron transmissions ($\frac{T_n}{T_{n0}}$) as a function of neutron energy.

in Fig. 8. The ratio of the neutron transmission in the energy region from 1 meV to 10 eV is shown in Supplementary Fig. S3.

Figure 9(a) shows $\sigma_p P$, which is calculated from the ratio of the neutron transmission T_n/T_{n0} (Fig. 8) and Eq. (4). The error of $\sigma_p P$ includes the statistical error of transmitted neutrons and the filter thickness of 4.1 ± 0.1 mm. By dividing $\sigma_p P$ in Fig. 9(a) by the literature value of σ_p, the absolute value of the proton polarization is calculated. The absolute value is only obtained in the energy region of 0.1–10 eV because the neutron–proton scattering cross-section is practically constant in the region higher than 0.1 eV, independent of filter material and temperature [34–38]. Thus, we applied the average value of σ_p at 0.1–10 eV in Ref. [5]. We obtained $P = 0.250 \pm 0.050$ as the average value in the beamtime. Figure 9(b) shows the neutron polarization P_n (white circle) and neutron transmission T_n (filled circle). The neutron transmission T_n (T_{n0}) is obtained by dividing the TOF spectrum of the polarized (unpolarized) naphthalene measurement by the TOF spectrum of the blank measurement. By substituting the transmission T_{n0} in Eq. (3), we obtained the cross-section of naphthalene (see Fig. 9(a)). Here, the number density of the naphthalene is 5.36×10^{21} cm^{-3}.

Figure 9(c) shows the FOM. The figures for the neutron energy region from 1 meV to 10 eV are shown in Supplementary Fig. S4. The average values at 0.1–10 eV were $P_n = 0.076 \pm 0.015$, $T_n = 0.555 \pm 0.001$, and FOM $= 0.0032 \pm 0.0009$. These results can be expected to be almost the same up to keV because of the flat neutron–proton scattering cross-section.

The quality of the polarized proton spin filter was judged in comparison with the polarized ^{3}He one. The FOM of the polarized ^{3}He case is defined in the same way as in Sect. 2. The difference from the proton case is that the ^{3}He cross-section is dominated by the capture cross-section, so the

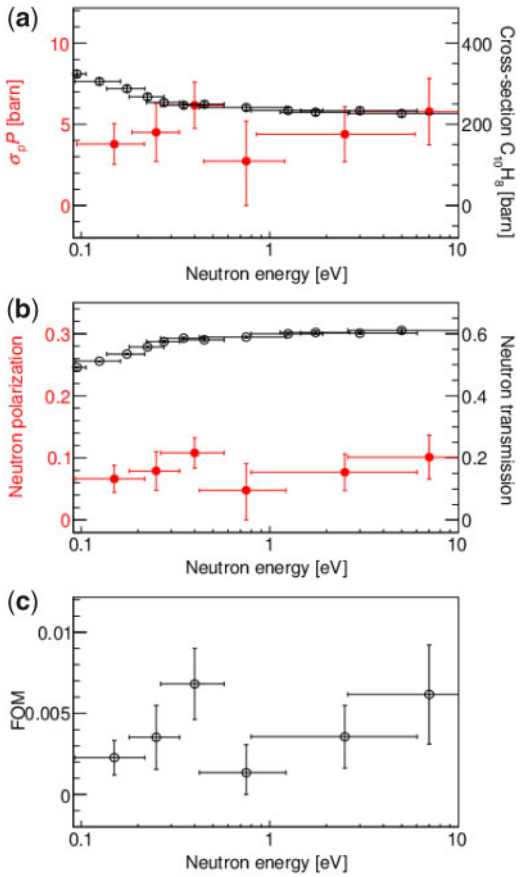

Fig. 9. (a) $\sigma_p P$ (filled circle) and the total cross-section of naphthalene (white circle). (b) Degree of neutron polarization (filled circle) and neutron transmission (white circle). (c) Figure of merit. These results were measured at 90 K and 0.35 T.

spin-dependent cross-section is given by the same value but the opposite sign as the capture cross-section. Assuming the performance of the polarized ^{3}He spin filter as ^{3}He polarization of 0.785, and a ^{3}He density of 41.5 bar cm [39], we determined that the FOM of our spin filter exceeds it at 120 eV. Further upgrades are necessary to achieve a higher FOM.

Increasing the thickness of the naphthalene crystal and the proton polarization is beneficial for improving the FOM. Higher proton polarization will be realized by cooling the chamber to a temperature lower than 90 K. According to the previous study by PSI, to apply DNP to naphthalene crystals at a temperature of 25 K increases the proton spin-lattice relaxation time to 800 hr and the proton polarization to 0.80 [11]. Increasing the laser power and enlarging the microwave resonator is necessary for polarizing a thicker spin filter. The laser intensity must be increased to irradiate the laser throughout the large filter. Increasing the laser intensity has the problem of exhausting the heat generated inside the crystal by absorbing the laser, but it can be cleared by the cooling. Also, enlargement of the microwave resonator means that the wavelength of the microwave becomes longer, which is equivalent to reducing the magnitude of the external magnetic field. Since the cooling will result in a sufficiently long relaxation time, the reduction of the relaxation time by lowering the magnetic field is much smaller. Therefore, all the necessary items for improving the FOM can be solved by lowering the temperature.

We will evaluate the performance of the improved spin filter. It is also intended to confirm that the performance yields the same values as those at 0.1–10 eV, even at higher neutron energies. We plan to halve the pulse width of the RANS proton beam for evaluation at higher energy. If the pulse width is reduced by half, it can be used up to 40 eV, but the statistics will also be halved. The lack of statistics due to the half pulse width is resolved by increasing the thickness of the ZnS(Li) scintillator of the RPMT detector. The detection efficiency of the scintillator of the RPMT detector, as stated in Sect. 3, is about 3% at 10 eV [33]. Using a 1 mm-thick scintillator increases the detection efficiency to about 8%. Even if the scintillator thickness is increased to 1 mm, the position resolution is acceptable.

5. Conclusions

We developed a novel triplet-DNP spin filter for the polarization of epithermal neutrons. Polarized epithermal neutrons are useful for studying compound states, which can answer open questions in physics. The triplet-DNP spin filter has the advantage of a milder environment than a polarized proton spin filter based on conventional DNP. Our spin filter, which is composed of a single cylindrical naphthalene crystal doped with 0.003 mol% of pentacene-d_{14}, has a size of $\varnothing 15 \times 4\,\mathrm{mm}^3$ and was operated at 0.35 T and 90 K. The performance of the triplet-DNP spin filter was evaluated using RANS. We succeeded in neutron polarization of the epithermal region. The proton polarization was 0.250 ± 0.050, while the neutron polarization was 0.076 ± 0.015 at 0.1–10 eV. The FOM of our spin filter exceeds that of ^{3}He at 10^2 eV. For future study, we will develop a larger spin filter which can be operated below 90 K to improve the FOM.

Acknowledgements

We especially thank the Advanced Manufacturing Support Team in RIKEN, who manufactured the microwave resonators. We are grateful to Shunsuke Endo, Atsushi Kimura, Takashi Ino, and NOPTREX collaboration for their constructive discussions. This work was supported by the RIKEN Incentive Research Projects.

Supplementary material

Supplementary data are available at *Progress of Theiretical and Experimental Physics* online.

References

[1] V. Gudkov and H. M. Shimizu, Phys. Rev. C **95**, 045501 (2017).
[2] V. P. Gudkov, Phys. Rep. **212**, 77 (1992).
[3] T. Okudaira et al., Phys. Rev. C **97**, 034622 (2018).
[4] G. E. Mitchell, J. D. Bowman, S. I. Penttilä, and E. I. Sharapov, Phys. Rep. **354**, 157 (2001).
[5] V. I. Luschikov, Y. V. Taran, and F. L. Shapiro, Sov. J. Nucl. Phys. **10**, 669 (1970).
[6] C. D. Jeffries, *Dynamic Nuclear Orientation*, (Interscience, New York, 1963).
[7] A. Abragam and M. Goldman, *Nuclear Magnetism: Order and Disorder*, (Clarendon Press, Oxford, 1982).
[8] M. Haag, B. van den Brandt, T. R. Eichhorn, P. Hautle, and W. T. Wenckebach, Nucl. Instrum. Meth. Phys. Res. Sect. A **678**, 91 (2012).
[9] T. R. Eichhorn, M. Haag, B. van den Brandt, P. Hautle, W. Th. Wenckebach, S. Jannin, J. J. van der Klink, and A. Comment, J. Magn. Reson. **234**, 58 (2013).
[10] T. R. Eichhorn, N. Niketic, B. van den Brandt, U. Filges, T. Panzner, E. Rantsiou, W. Th. Wenckebach, and P. Hautle, Nucl. Instrum. Meth. Phys. Res. Sect. A **754**, 10 (2014).
[11] Y. Quan, B. van den Brandt, J. Kohlbrecher, W. Th. Wenckebach, and P. Hautle, Nucl. Instrum. Meth. Phys. Res. Sect. A **921**, 22 (2019).
[12] N. Niketic, B. van den Brandt, W. Th. Wenckebach, J. Kohlbrecher, and P. Hautle, J. Appl. Crys. **48**, 1514 (2015).
[13] Y Otake et al., J. Disaster Res. **12**, 585 (2017).

[14] I. Gurevich and L. Tarasov, *Low Energy Neutron Physics*, (North-Holland Publishing Co., Amsterdam, 1968).
[15] H. Glättli and M. Goldman, *Methods of Experimental Physics*, (Academic Press, New York, 1987).
[16] H Börner et al., *Neutron Data Booklet*, (OCP Science, Philadelphia, PA, 2003).
[17] W. G. Williams, *Polarized Neutrons*, (Clarendon Press, Oxford, 1988).
[18] A. Henstra, T.-S. Lin, J. Schmidt, and W. Th. Wenckebach, Chem. Phys. Lett. **165**, 6 (1990).
[19] K. Tateishi, M. Negoro, S. Nishida, A. Kagawa, Y. Morita, and M. Kitagawa, Proc. Nat. Acad. Sci. **111**, 7527 (2014).
[20] K. Tateishi, M. Negoro, A. Kagawa, and M. Kitagawa, Angew. Chem. Inter. Ed. **52**, 13307 (2013).
[21] M. Negoro, A. Kagawa, K. Tateishi, Y. Tanaka, T. Yuasa, K. Takahashi, and M. Kitagawa, J. Phys. Chem. A **122**, 4294 (2018).
[22] S. Fujiwara, M. Hosoyamada, K. Tateishi, T. Uesaka, K. Ideta, N. Kimizuka, and N. Yanai, J. Am. Chem. Soc. **140**, 15606 (2018).
[23] T. R. Eichhorn, B. van den Brandt, P. Hautle, A. Henstra, and W. Th. Wenckebach, Mol. Phys. **112**, 1773 (2014).
[24] A. J. Van Strien and J. Schmidt, Chem. Phys. Lett. **70**, 513 (1980).
[25] A. Henstra and W. Th. Wenckebach, Mol. Phys. **112**, 1761 (2014).
[26] K. Takeda, Rev. Sci Instrum. **78**, 033103 (2007).
[27] K. Takeda, J. Magn. Reson. **192**, 218 (2008).
[28] M. Takamura, Y. Ikeda, H. Sunaga, A. Taketani, Y. Otake, H. Suzuki, M. Kumagai, T. Hama, and Y. Oba, J. Phys. Conf. Ser. **734**, 032047 (2016).
[29] Y. Ikeda, Y. Otake, and M. Mizuta, J. Adv. Concr. Technol. **15**, 603 (2017).
[30] A Taketani et al., ISIJ Int. **57**, 155 (2017).
[31] Y. Wakabayashi, Y. Yoshimura, M. Mizuta, Y. Otake, and Y. Ikeda, J. Adv. Concr. Technol. **17**, 571 (2019).
[32] Y. Yoshimura, M. Mizuta, H. Sunaga, Y. Otake, and Y. Ishikawa, JAILCD, 233 (2019).
[33] S. Satoh, Plasma Fusion Res. **13**, 2405056 (2018).
[34] J. R. Granada, Z. Naturforsch. A **39**, 1160 (1984).
[35] G. L. Squires, *Introduction to the Theory of Thermal Neutron Scattering*, (Cambridge University Press, Cambridge, 2012).
[36] M. Mattes and E. Sartori, *Jef-1 Scattering Law Data*, (Nuclear Energy Agency, Paris, 1984).
[37] S. Grieger, H. Friedrich, K. Guckelsberger, R. Scherm, and W. Press, J. Chem. Phys. **109**, 3161 (1998).
[38] N. Morishima and Y. Sakurai, Nucl. Instrum. Meth. Phys. Res. Sect. A **490**, 527 (2002).
[39] Z. Salhi et al., J. Phys.: Conf. Ser. **1316**, 012009 (2019).